A Single-Switch AC–DC LED Driver Based on a Boost-Flyback PFC Converter With Lossless Snubber

Sin-Woo Lee and Hyun-Lark Do

***Abstract*—A single-switch ac–dc light-emitting-diode (LED) driver based on boost-flyback power factor correction (PFC) converter with a lossless snubber is proposed. In the proposed LED driver, the boost PFC module is designed to be operated in the discontinuous-conduction mode to achieve a high power factor. The dc–dc flyback module is designed to provide input–output electrical isolation to improve safety. The lossless snubber circuit clamps the peak voltage spike of switch to a low voltage and the leakage inductor energy is recycled via the dc–dc flyback module. Additionally, a low-voltage-rating capacitor can be used as the dc-bus capacitor because some of the input power is directly conducted to the output; the remaining power is stored in the dc-bus capacitor. Therefore, the proposed LED driver can provide a high power factor and a high power conversion efficiency. These results are verified for an output of 48 V and 2 A for the experimental prototype.**

***Index Terms*—Boost-flyback converter, LED driver, lossless snubber, power factor correction (PFC).**

I. Introduction

RECENTLY, with the advances in light-emitting-diode (LED) technology, LEDs have drawn much interest in a wide range of lighting applications. Compared to conventional lighting device such as fluorescent lamps, LEDs have many advantages: lower power consumption, longer lifetimes (typically 80 000 h), higher optical efficiency, higher contrast ratios and superior environmental safety [1]–[5]. Therefore, many studies of LED drivers (to replace conventional fluorescent lamp systems) have been produced. To operate LEDs, ac–dc or dc–dc converters are used in LED drivers to satisfy the demand for high efficiency, low cost, and low size. Especially, for an ac input voltage, the active power factor correction (PFC) circuit must produce little harmonic pollution and a high power factor.

To achieve electrical isolation to improve safety, the conventional flyback converter is widely used in LED drivers. However, an additional RCD snubber is needed because of high voltage spikes from the main switch because the leakage inductance resonates with the parasitic output capacitance of the MOSFETs [6]–[12]. The flyback LED driver in [9] was proposed to reduce switching losses and recycle the leakage inductor energy. Another flyback LED driver, which has low voltage stress and low output current ripple because of its interleaved structure, was proposed in [11]. However, this driver has several drawbacks such as requiring many components, a large size, and complex control. Neither of these LED drivers is suitable for tightly regulated output voltage because of the absence of a buffer capacitor. Most single-stage converters do not have a buffer capacitor.

Two-stage-type LED drivers are suitable for tightly controlled output voltages because they utilize a dc-bus capacitor, which reduces the difference between the input power and the output power [12]. However, these LED drivers have two switches and two control circuits in each stage; therefore, they are usually large size, have a large components, are more expensive, and are less energy efficient. To overcome these problems, the two-stage LED driver is modified to become a single-stage LED driver by sharing a switch with both stages [13]–[18]. A boost or buck–boost converter for PFC and a flyback converter are integrated in a single stage in [13]–[15]. Boost and a buck–boost PFC circuits are widely used because they can provide a high power factors using a simple structure and a simple control circuit. In [16]–[18], several single-stage LED drivers, which use half-bridge *LLC* converters at the dc–dc stage, are presented. In the half-bridge *LLC* converter, soft-switching operation of the power switches reduces switching loss and increases efficiency.

In this paper, a single-stage ac–dc LED driver based on a boost-flyback PFC converter with a lossless snubber is proposed. Because the proposed LED driver is based on the boost-flyback structure, it achieves a high power factor based on the boost PFC, which is operated in the discontinuous-conduction mode (DCM). Additionally, the proposed LED driver provides electrical isolation due to the dc–dc flyback module. And, because the lossless snubber circuit is used, the leakage inductor energy is recycled into the dc–dc flyback circuit and the peak voltage spike in the main switch is clamped to a low voltage. Moreover, the dc-bus capacitor is divided into two capacitors, i.e., the snubber capacitor and another dc-bus capacitor. Additionally, some of the input power is directly delivered to the output; the remaining power is stored through the snubber diode. Hence, the energy conversion efficiency is improved and a voltage of dc-bus capacitor is also reduced. In conclusion, the proposed LED driver can provide a high power factor and achieve a high power conversion efficiency. A theoretical analysis and an experimental prototype of the proposed LED driver are presented to verify the PFC and efficiency improvement.

Manuscript received September 24, 2015; revised December 8, 2015 and February 10, 2016; accepted March 28, 2016. Date of publication March 31, 2016; date of current version November 11, 2016. Recommended for publication by Associate Editor R.-L. Lin. This work was supported by the Human Resources Development of the Korea Institute of Energy Technology Evaluation and Planning Grant funded by the Korea government Ministry of Trade, Industry & Energy (20154030200720).

The authors are with the Department of Electronic & Information Engineering, Seoul National University of Science and Technology, Seoul 139-743, South Korea (e-mail: weaerz@gmail.com; hldo@ snut.ac.kr).

Color versions of one or more of the figures in this paper are available online at http://ieeexplore.ieee.org.

Digital Object Identifier 10.1109/TPEL.2016.2549029

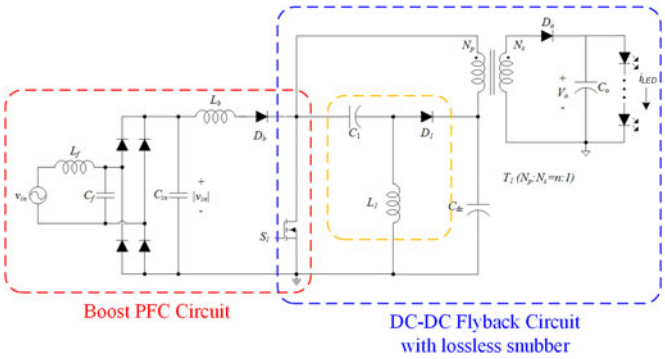

Fig. 1. Circuit diagram of the proposed LED driver.

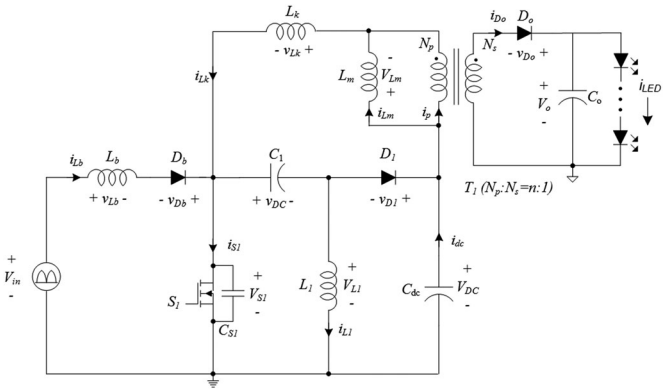

Fig. 2. Equivalent circuit diagram of the proposed LED driver.

II. Operating Principle

A. Circuit Description

A circuit diagram of the proposed LED driver is shown in Fig. 1. The input line filter consists of L_f and C_f. The boost PFC circuit is composed of the boost inductor L_b, the main switch S_1, and the reverse-blocking diode D_b (which blocks reverse current through the boost inductor for DCM operation). The dc–dc flyback circuit includes the coupled inductor T_1, the shared (common) switch S_1, the dc-bus capacitor $C_{\rm dc}$, the output diode D_o, the output capacitor C_o, and the lossless snubber circuit composed of L_1, C_1, and D_1.

In order to describe to parasitic component of circuit parts for theoretical analysis, an equivalent circuit diagram of the proposed LED driver is shown in Fig. 2 (the input line filters and the bridge diode are not included). The input voltage is expressed as the rectified line voltage $V_{\rm in}$; it is considered to be constant value during a switching period. The capacitor C_{S1} is the parasitic output capacitance of S_1. The coupled inductor T_1 has a magnetizing inductor L_m and a leakage inductor L_k with a turn ratio of n:1 ($n = N_p/N_s$). L_k is assumed to be much smaller than the L_m. According to the volt–second balance law, since the average inductor voltage should be zero at the steady state, the voltages across the C_1 and $C_{\rm dc}$ should be equal to $V_{\rm dc}$. The capacitances of C_1, $C_{\rm dc}$, and C_o are large enough that their voltages are considered to be constant.

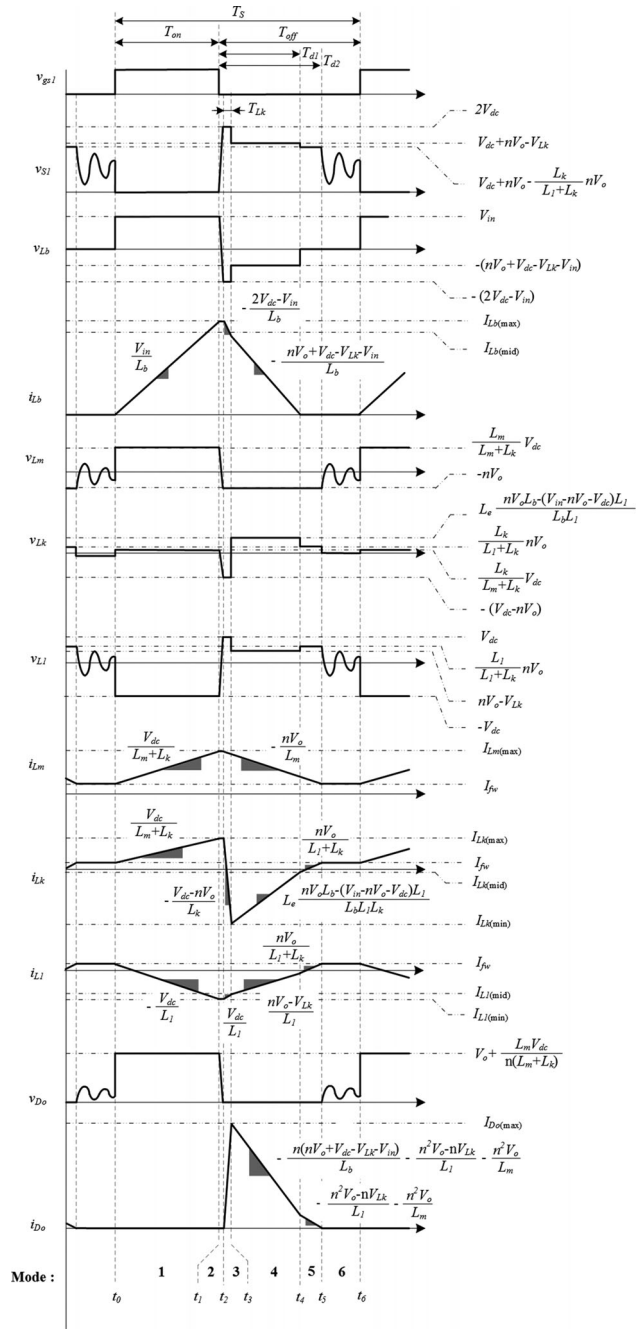

Fig. 3. Key waveforms of the proposed LED driver.

B. Model Analysis

Figs. 3 and 4 show the theoretical waveforms and operating modes of the proposed LED driver during a switching period T_s which can be divided into six operating modes.

Before t_0, the main switch S_1 and the output diode D_o are turned off. The parasitic output capacitance of S_1 is discharged because of the drain-source voltage oscillation between $(L_m + L_k)//L_1$ and C_{S1}. The magnetizing inductor current $i_{\rm Lm}$ and the snubber inductor current i_{L1} are the same as the freewheeling current $i_{\rm fw}$ (which is a constant).

Mode 1 $[t_0, t_1]$: At t_0, S_1 is turned on and D_o is reverse-biased. Therefore, the boost inductor voltage $V_{\rm Lb}$ is equal to $V_{\rm in}$. $i_{\rm Lb}$

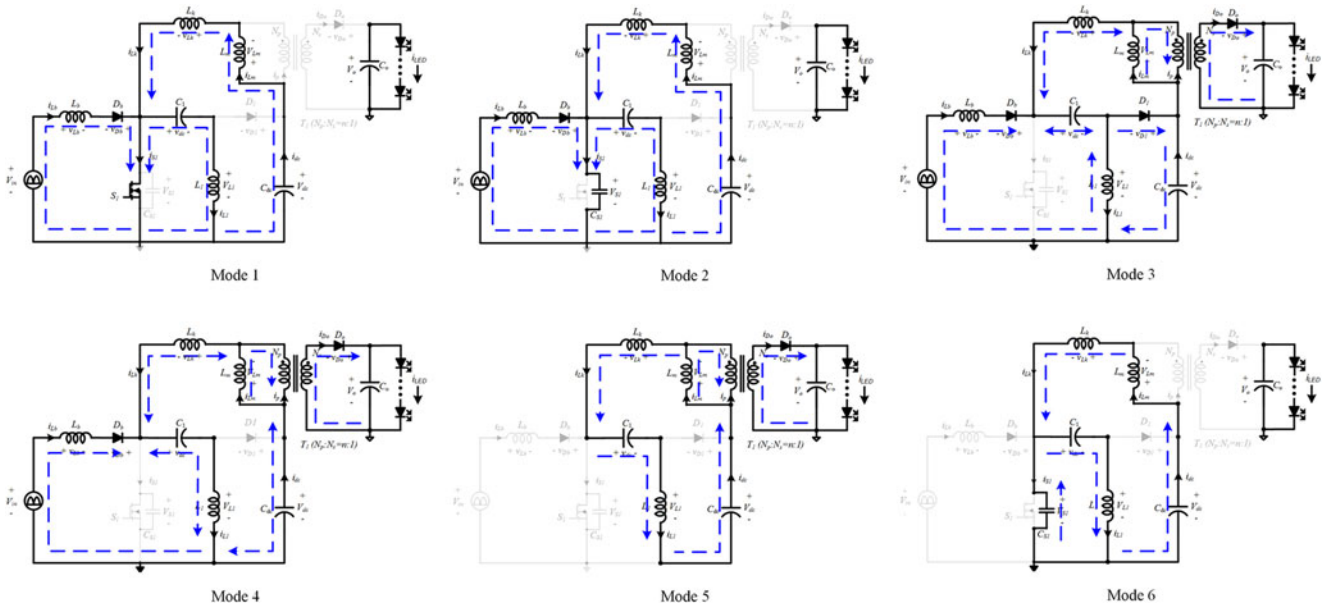

Fig. 4. Operating modes.

can be derived as follows:

$$i_{\mathrm{Lb}}(t) = \frac{V_{\mathrm{in}}}{L_b}(t - t_0). \tag{1}$$

The total voltage across both components L_m and L_k is V_{dc}. Therefore, the voltage V_{dc} is divided into V_{Lm} and V_{Lk}, which are given by $V_{\mathrm{dc}}L_m/(L_m + L_k)$ and $V_{\mathrm{dc}}L_k/(L_m + L_k)$, respectively. i_{Lm} and i_{Lk} can be obtained using

$$i_{\mathrm{Lm}}(t) = i_{\mathrm{Lk}}(t) = I_{\mathrm{fw}} + \frac{V_{\mathrm{dc}}}{L_m + L_k}(t - t_0). \tag{2}$$

The snubber inductor voltage V_{L1} is equal to $-V_{\mathrm{dc}}$. i_{L1} can be derived as follows:

$$i_{L1}(t) = I_{\mathrm{fw}} + \frac{-V_{\mathrm{dc}}}{L_1}(t - t_0). \tag{3}$$

At the end of this mode, i_{Lb}, i_{Lm}, i_{Lk}, and i_{L1} arrive at the maximum or minimum current as follows:

$$I_{\mathrm{Lb(max)}} = \frac{V_{\mathrm{in}}}{L_b}T_{\mathrm{on}} \tag{4}$$

$$I_{\mathrm{Lm(max)}} = I_{\mathrm{Lk(max)}} = I_{\mathrm{fw}} + \frac{V_{\mathrm{dc}}}{L_m + L_k}T_{\mathrm{on}} \tag{5}$$

$$I_{L1(\mathrm{min})} = I_{\mathrm{fw}} + \frac{-V_{\mathrm{dc}}}{L_1}T_{\mathrm{on}} \tag{6}$$

where T_{on} is the turn-on time which is the time interval between t_0 and t_1.

Mode 2 [t_1, t_2]: At t_1, S_1 is turned off and the parasitic output capacitor C_{S1} begins to charge. Because C_{S1} is assumed to be very small, the interval between t_1 and t_2 is very short. i_{Lb}, i_{Lm}, and i_{L1} are considered to remain at constant values; ($i_{\mathrm{Lb(max)}}$, $i_{\mathrm{Lm(max)}}$, and $i_{L1(\mathrm{min})}$, respectively). V_{Lb}, V_{Lm}, and V_{L1} are considered to linearly increase with very large slops.

Mode 3 [t_2, t_3]: At t_2, when C_{S1} charges up to $2V_{\mathrm{dc}}$, the snubber diode D_1 is forward biased and begins to conduct. Therefore, the main switch voltage V_{S1} is clamped to $2V_{\mathrm{dc}}$ by D_1. The current flowing into D_1 is determined by $i_{\mathrm{Lb}} + i_{\mathrm{Lk}}$-$i_{L1}$. In this mode, the current of leakage inductor is absorbed by the capacitors C_1 and C_{dc}. Since L_k is assumed to be very small, the time interval between t_2 and t_3 is short.

Because V_{Lb} is given by $-(2V_{\mathrm{dc}} - V_{\mathrm{in}})$, i_{Lb} can be derived as follows:

$$i_{\mathrm{Lb}}(t) = I_{\mathrm{Lb(max)}} + \frac{-(2V_{\mathrm{dc}} - V_{\mathrm{in}})}{L_b}(t - t_2). \tag{7}$$

V_{Lm} and V_{Lk} are $-nV_o$ and $-(V_{\mathrm{dc}} - nV_o)$, respectively. Therefore, i_{Lm} and i_{L1} can be obtained using

$$i_{\mathrm{Lm}}(t) = I_{\mathrm{Lm(max)}} + \frac{-nV_o}{L_m}(t - t_2) \tag{8}$$

$$i_{\mathrm{Lk}}(t) = i_{\mathrm{Lk(max)}} + \frac{-(V_{\mathrm{dc}} - nV_o)}{L_k}(t - t_2). \tag{9}$$

Because V_{L1} is V_{dc}, i_{L1} can be derived as follows:

$$i_{L1}(t) = i_{L1(\mathrm{min})} + \frac{V_{\mathrm{dc}}}{L_1}(t - t_2). \tag{10}$$

At the end of this mode, i_{Lb}, i_{Lk}, and i_{L1} arrive at middle or minimum currents as follows:

$$I_{\mathrm{Lb(mid)}} = I_{\mathrm{Lb(max)}} + \frac{-(2V_{\mathrm{dc}} - V_{\mathrm{in}})}{L_b}T_{\mathrm{Lk}} \tag{11}$$

$$I_{\mathrm{Lk(min)}} = I_{\mathrm{Lk(max)}} + \frac{-(V_{\mathrm{dc}} - nV_o)}{L_k}T_{\mathrm{Lk}} \tag{12}$$

$$I_{L1(\mathrm{mid})} = I_{L1(\mathrm{min})} + \frac{V_{\mathrm{dc}}}{L_1}T_{\mathrm{Lk}} \tag{13}$$

where T_{Lk} is the leakage inductor discharging time, which is the time interval between t_2 and t_3.

Because the output diode D_o is turned on in this mode, i_{Do} arrives at the maximum current with a very large

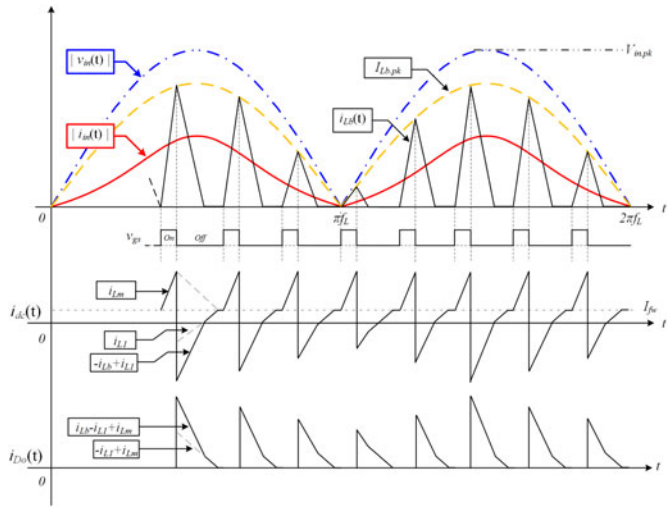

Fig. 5. Theoretical waveforms of rectified input line voltage, input current, boost inductor current, dc-bus capacitor current and output current in a line period.

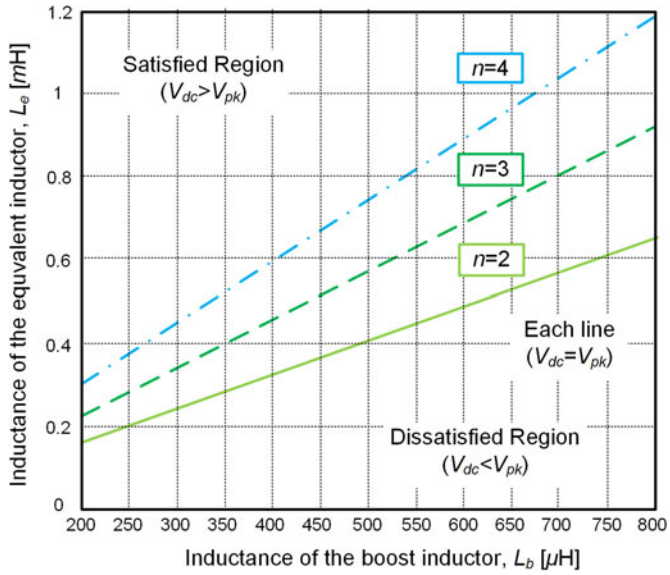

Fig. 6. Relationship between L_b and L_e according to turn ratio n.

slope as follows:

$$I_{\mathrm{Do(max)}} = n\left(I_{\mathrm{Lm(max)}} + \frac{-nV_o}{L_m}T_{\mathrm{Lk}} - I_{\mathrm{Lk(min)}}\right). \quad (14)$$

Mode 4 [t_3, t_4]: When D_1 is turned off, this mode starts. In this mode, V_{Lb}, V_{L1} and V_{Lk} are expressed as follows:

$$V_{\mathrm{Lb}} = -(nV_o + V_{\mathrm{dc}} - V_{\mathrm{Lk}} - V_{\mathrm{in}}) \quad (15)$$

$$V_{L1} = nV_o - V_{\mathrm{Lk}} \quad (16)$$

$$V_{\mathrm{Lk}} = L_s\frac{nV_oL_b - (V_{\mathrm{in}} - nV_o - V_{\mathrm{dc}})L_1}{L_bL_1} \quad (17)$$

where $1/L_s = (1/L_k) + (1/L_1) + (1/L_b)$.

TABLE I
VOLTAGE AND CURRENT STRESS ON THE COMPONENTS OF THE PROPOSED LED DRIVER

Component	Voltage stress	Current stress
S_1	$2V_{\mathrm{dc}}$	$I_{\mathrm{Lb(max)}} + I_{\mathrm{Lm(max)}} - I_{L1\mathrm{(min)}}$
D_b	$V_{\mathrm{dc}} + nV_o - V_{\mathrm{in}}$	$I_{\mathrm{Lb(max)}}$
D_1	$2V_{\mathrm{dc}}$	$I_{\mathrm{Lb(max)}} - I_{L1\mathrm{(min)}}$
D_o	$V_o + V_{\mathrm{dc}}/n$	$n(I_{\mathrm{Lb(max)}} + I_{\mathrm{Lm(max)}} - I_{L1\mathrm{(min)}})$

i_{Lb}, i_{L1}, and i_{Lk} can be obtained using

$$i_{\mathrm{Lb}}(t) = I_{\mathrm{Lb(mid)}} + \frac{-(nV_o + V_{\mathrm{dc}} - V_{\mathrm{Lk}} - V_{\mathrm{in}})}{L_b} \times (t - t_3) \quad (18)$$

$$i_{L1}(t) = I_{L1\mathrm{(mid)}} + \frac{nV_o - V_{\mathrm{Lk}}}{L_1}(t - t_3) \quad (19)$$

$$i_{\mathrm{Lk}}(t) = I_{\mathrm{Lk(min)}} + L_s\frac{nV_oL_b - (V_{\mathrm{in}} - nV_o - V_{\mathrm{dc}})L_1}{L_bL_1L_k} \times (t - t_3). \quad (20)$$

At the end of this mode, i_{Lk} arrives at each middle current as follows:

$$I_{\mathrm{Lk(mid)}} = I_{\mathrm{Lk}}(t_4). \quad (21)$$

Then, i_{Lb}, i_{L1}, and i_{Lm} flow through the coupled inductor T_1 to the secondary side. Thus, the output diode current i_{Do} is expressed as follows:

$$i_{\mathrm{Do}}(t) = I_{\mathrm{Do(max)}} + n\left\{\frac{-(nV_o + V_{\mathrm{dc}} - V_{\mathrm{Lk}} - V_{\mathrm{in}})}{L_b} + \frac{-nV_o + V_{\mathrm{Lk}}}{L_1} + \frac{-nV_o}{L_m}\right\}(t - t_3). \quad (22)$$

Equation (22) shows that the boost inductor current i_{Lb} flows through the coupled inductor T_1 to the output diode D_o. Therefore, some of the input power is directly delivered to the load.

Mode 5 [t_4, t_5]: At t_4, the boost inductor current i_{Lb} reaches zero. Therefore, the reverse-current-blocking diode D_b is turned off. Thus, the output diode current i_{Do} decreases linearly with a slope of $-(nV_o + V_{\mathrm{Lk}})/L_1 - nV_o/L_m$.

The voltage nV_o is divided into V_{L1} and V_{Lk}, which are nV_o $L_1/(L_1 + L_k)$ and nV_o $L_k/(L_1 + L_k)$, because the total voltage across both components L_1 and L_k is equal to nV_o. i_{L1} and i_{Lk} can be obtained using

$$i_{L1}(t) = i_{\mathrm{Lk}}(t) = I_{\mathrm{Lk(mid)}} + \frac{nV_o}{L_1 + L_k}(t - t_4). \quad (23)$$

At the end of this mode, i_{Lm}, i_{Lk}, and i_{L1} arrive at the freewheeling current as follows:

$$I_{\mathrm{fw}} = I_{\mathrm{Lm}}(t_5) = I_{\mathrm{Lk}}(t_5) = I_{L1}(t_5). \quad (24)$$

Mode 6 [t_5, t_6]: When the output diode current i_{Do} reaches zero, this mode starts. Therefore, the output diode D_o is turned off. In this mode, the freewheeling current I_{fw} flows through L_k, C_1, L_1, C_{dc}, and L_m. Then, V_{S1} nonlinearly decreases with the oscillation between C_{S1} and $L_1//(L_m + L_k)$.

TABLE II
SELECTED PARAMETERS AND COMPONENTS OF THE LABORATORY PROTOTYPE

Component		Value	Description
Input filter	L_f	1.29 mH	EI3329S, Liz wire (32/φ0.12)
	C_f	0.1 μF	630 V
Input capacitor, $C_{\rm in}$		0.57 μF	630 V
Bridge diode, $D_{\rm bridge}$		BR-KBL406	600 V/4 A
Boost inductor, L_b		350 μH	EI3329S, Lizwire (32/φ0.12)
Revers-blocking diode, D_b		RHRP3060	600 V/30 A ultra-fast diode
Main switch, S_1		SPP20N60C3	650 V/20.7 A, $R_{\rm ds\_on=0.19\ \Omega}$
Snubber circuit	D_1	BYR29X-800	800 V/8 A ultra-fast diode
	L_1	761 μH	EI3329S, Liz wire (32/φ0.12)
	C_1	47 μF	450 V
DC-Bus capacitor, $C_{\rm dc}$		47 μF	450 V
Coupled inductor, T_1		L_m = 758 μH L_k = 1 μH N_p :N_s :N_a = 48T:16T:6T	EI3329S, Liz wire (15/φ0.10)N_1 \!, (32/φ0.12)N_1 \!,N_a
Output diode, D_o		RF2001T3D	300 V/20 A ultra-fast diode
Output capacitor, C_o		470 μF x3	100 V
Control IC		KA7552	PWM controller
Two linear constant LED current circuit	S_{d1}, S_{d2}	IRF540	100 V/28 A, $R_{\rm ds_{on}} = 0.077\ \Omega$
	Op-Amp	LM2904	Dual operational amplifier
LED module		LS-P5W11-H-STAR	5 W, White, CCT:5500

III. DESIGN PROCEDURE

To simplify mathematical analysis for the design procedure, the leakage inductor L_k and the parasitic output capacitor C_{S1}, which have small enough to be ignored, are not considered.

A. Input Current and Power Factor

The theoretical waveforms of rectified input line voltage $|v_{\rm in}(t)|$, rectified input current $|i_{\rm in}(t)|$, and boost inductor current $i_{\rm Lb}(t)$ in one line period are shown in Fig. 5. The line voltage $v_{\rm in}(t)$ is given by

$$v_{\rm in}(t) = V_{\rm in.pk}\sin(2\pi f_L t) \tag{25}$$

where the $V_{\rm in.pk}$ is the peak input voltage and f_L is the line frequency. To simplify the notation, phase angle ωt can be substituted for $2\pi f_L$.

In Fig. 5, the boost inductor L_b operates in DCM with constant duty during one line period. The peak boost inductor current $i_{\rm Lb.pk}(t)$, which follows the input line voltage $v_{\rm in}(t)$ can be obtained using

$$I_{\rm Lb.pk} = \frac{V_{\rm in}(t)}{L_b}T_{\rm on} = \frac{nV_o + V_{\rm dc} - V_{\rm in}(t)}{L_b}T_{d1} \tag{26}$$

where $V_{\rm in}(t)$ is the rectified line voltage $|v_{\rm in}(t)|$, and T_{d1} is the discharging time of the boost inductor which is the interval between t_1 and t_4. $T_{\rm on}$ has a constant value (because of the fixed duty ratio during one line period) to supply the output power for a constant output voltage. From (26), T_{d1} is obtained using

$$T_{d1} = \frac{V_{\rm in}(t)}{nV_o + V_{\rm dc} - V_{\rm in}(t)}DT_S \tag{27}$$

where $D(= T_{\rm on}/T_s)$ is the duty cycle.

The input current $i_{\rm in}(t)$ is the average boost inductor current $i_{\rm Lb.avg}(t)$ during the switching period T_s as follows:

$$\begin{aligned} i_{\rm in}(t) &= i_{\rm Lb.avg}(t) = i_{\rm Lb(Ton).avg} + i_{\rm Lb(Td1).avg} \\ &= \frac{1}{2}I_{\rm Lb.pk}\frac{(T_{\rm on}+T_{d1})}{T_s} \\ &= \frac{V_{\rm in.pk}D^2T_s}{2L_b}\frac{|\sin(\omega t)|}{1-\frac{V_{\rm in.pk}}{V_{\rm dc}+nV_o}|\sin(\omega t)|}. \end{aligned} \tag{28}$$

The average input power in a half-line cycle can be calculated as

$$\begin{aligned} P_{\rm in} &= \frac{1}{\pi}\int_0^\pi v_{\rm in}(t)i_{\rm in}(t)dt = \frac{{V_{\rm in.pk}}^2D^2T_s}{2\pi L_b} \\ &\times \int_0^\pi \frac{\sin^2(\omega t)}{1-\frac{V_{\rm in.pk}}{V_{\rm dc}+nV_o}|\sin(\omega t)|}d\omega t. \end{aligned} \tag{29}$$

The power factor can be expressed as

$$PF = \frac{P_{\rm in}}{V_{\rm rms}I_{\rm rms}} = \frac{\sqrt{2}P_{\rm in}}{V_{\rm in.pk}\sqrt{\frac{1}{\pi}\int_0^\pi {i_{\rm in}}^2(t)dt}}. \tag{30}$$

where $V_{\rm rms}$ and $I_{\rm rms}$ are the RMS values of the input voltage and current, respectively.

B. Output Current

To obtain T_{d2}, the maximum magnetizing inductor current $I_{\rm Lm.(max)}$ is given by

$$I_{\rm Lm(max)} = I_{\rm fw} + \frac{V_{\rm dc}}{L_m}T_{\rm on} = I_{\rm fw} + \frac{nV_o}{L_m}T_{d2} \tag{31}$$

$$T_{d2} = \frac{V_{\rm dc}}{nV_o}DT_s \le T_{\rm off} = (1-D)T_s. \tag{32}$$

From (32), the following equation can be obtained:

$$D \le \frac{nV_o}{nV_o + V_{\rm dc}}. \tag{33}$$

The output diode current $i_{\rm Do}(t)$ for one line period is shown in Fig. 5. The output current I_o is the average output diode D_o

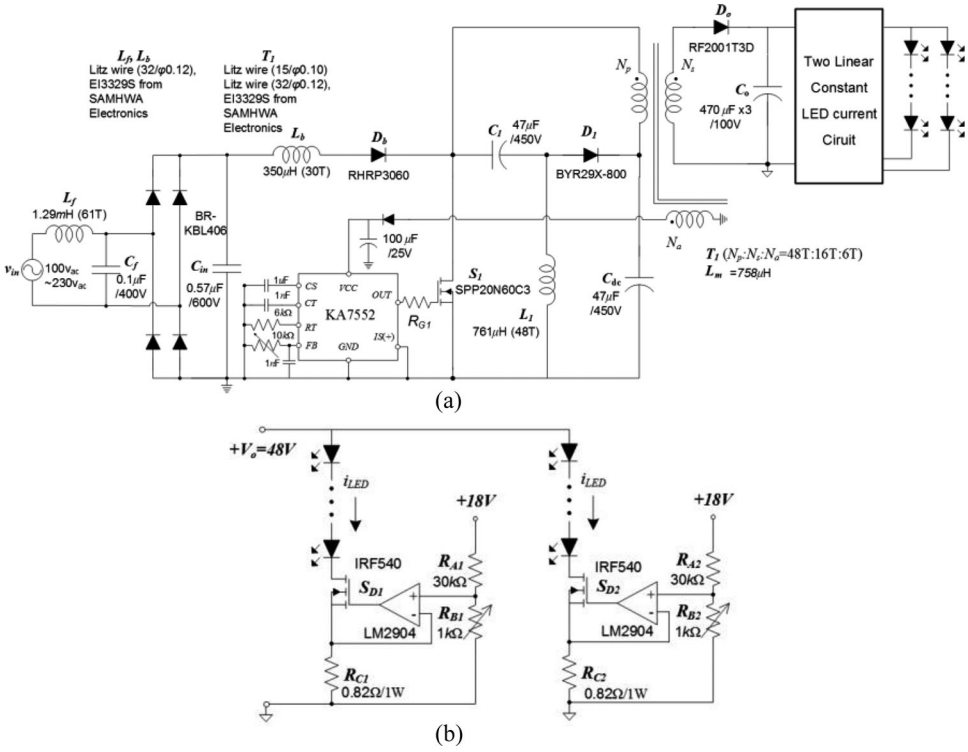

Fig. 7. Laboratory prototype circuit diagram of the proposed LED driver. (a) Laboratory prototype ac–dc circuit diagram. (b) Two linear constant LED current circuit.

current $i_{\mathrm{do.avg}}(t)$ in the half-line period which is expressed as

$$I_o = i_{\mathrm{Do.avg}}(t) = \frac{1}{\pi}\int_0^{\pi} n(i_{\mathrm{Lb(Td1).avg}} - i_{L1(\mathrm{Td2}).\mathrm{avg}} + i_{\mathrm{Lm(Td2).avg}})dt = \frac{n{V_{\mathrm{in.pk}}}^2 D^2 T_s}{2\pi L_b} \times \int_0^{\pi} \frac{\sin^2(\omega t)}{V_{\mathrm{dc}} + nV_o - V_{\mathrm{in.pk}}|\sin(\omega t)|}d\omega t + \frac{{V_{\mathrm{dc}}}^2}{4V_o L_1}D^2 T_s + \frac{{V_{\mathrm{dc}}}^2}{4V_o L_m}D^2 T_s. \quad (34)$$

C. Analysis of the DC-Bus Voltage

The dc-bus capacitor current $i_{\mathrm{dc}}(t)$ for one line period is shown in Fig. 5. This current consists of i_{Lm}, i_{Lb}, and i_{L1} in one switching period T_s.

The average dc-bus capacitor current $i_{\mathrm{dc.avg}}(t)$ in the half-line period is expressed as

$$i_{\mathrm{dc.avg}}(t) = \frac{1}{\pi}\int_0^{\pi}(i_{\mathrm{Lm(Ton).avg}} - i_{\mathrm{Lb(Td1).avg}} + i_{L1(\mathrm{Td2}).\mathrm{avg}} - I_{\mathrm{fw}})dt = I_{\mathrm{fw}} + \frac{V_{\mathrm{dc}}}{2L_m}D^2 T_s - \frac{{V_{\mathrm{in.pk}}}^2 D^2 T_s}{2\pi L_b} \times \int_0^{\pi} \frac{\sin^2(\omega t)}{V_{\mathrm{dc}} + nV_o - V_{\mathrm{in.pk}}|\sin(\omega t)|}d\omega t + \frac{-{V_{\mathrm{dc}}}^2}{4nV_o L_1}D^2 T_s = 0. \quad (35)$$

From (35), I_{fw} can be obtained. Because $i_{\mathrm{dc.avg}}(t)$ should be zero, V_{dc} has a constant value that is always higher than $V_{\mathrm{in.pk}}$ because of the structure of the boost converter in the PFC circuit.

From (29), (34), and (35), assuming that P_{in} is equal to P_o, and following equation can be obtained:

$$V_{\mathrm{dc}} = \frac{2{V_{\mathrm{in.pk}}}^2 L_e}{\pi L_b(V_{\mathrm{dc}} + nV_o)} \times \int_0^{\pi} \frac{\sin^2(\omega t)}{1 - \frac{V_{\mathrm{in.pk}}}{V_{\mathrm{dc}}+nV_o}|\sin(\omega t)|}d\omega t. \quad (36)$$

where $1/L_e = (1/L_1) + (1/L_m)$.

Equation (36) shows that V_{dc} is not influenced by the load condition.

D. Design of the Inductors L_b, L_1, and L_m

From (29), assuming that the efficiency of the proposed LED driver is 100%, i.e., $P_{\mathrm{in}} = P_o$, the boost inductor L_b should be determined as

$$L_b = \frac{{V_{\mathrm{in.pk}}}^2 D^2}{2\pi P_o f_s}\int_0^{\pi} \frac{\sin^2(\omega t)}{1 - \frac{V_{\mathrm{in.pk}}}{V_{\mathrm{dc}}+nV_o}|\sin(\omega t)|}d\omega t \quad (37)$$

where f_s is the switching frequency. By substituting $n = 3$, $V_{\mathrm{pk}} = 100\sqrt{2}$ V, $V_{\mathrm{dc}} = V_{\mathrm{pk}}$ [V], $f_s = 50$ kHz, $P_o = 100$ W and $D = 0.45$ in (37); thus, $L_b = 355$ μH is obtained.

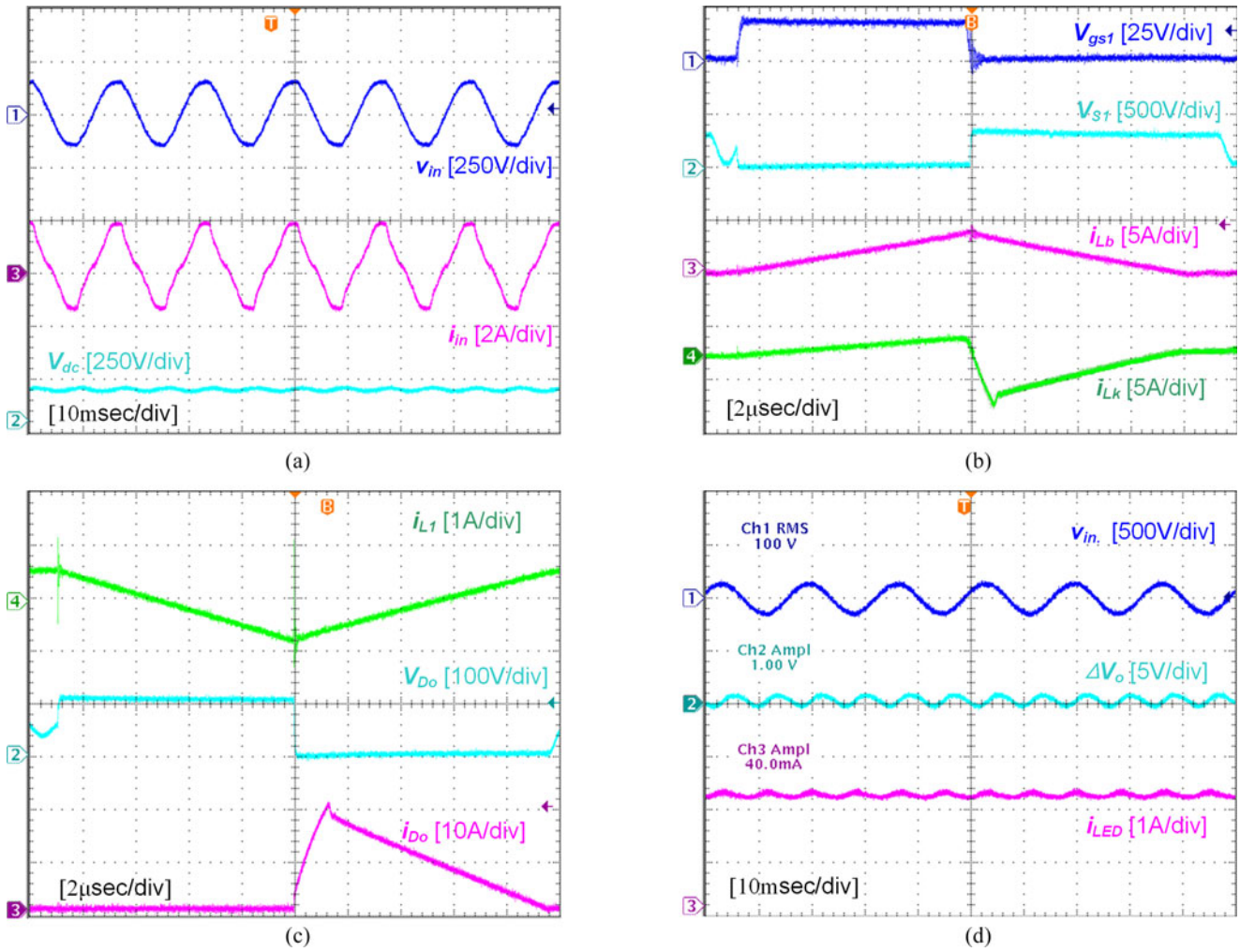

Fig. 8. Experimental waveforms at $v_{\rm in} = 100[V_{\rm ac}]$. (a) $v_{\rm in}$, $i_{\rm in}$, and $V_{\rm dc}$, (b) $v_{\rm gs1}$, v_{S1}, $i_{\rm Lb}$, and $i_{\rm Lk}$, (c) i_{L1}, $v_{\rm Do}$, and $i_{\rm Do}$, (d) $v_{\rm in}$, ΔV_o, and $i_{\rm LED}$.

From (36), L_e can be determined as

$$L_e = \frac{V_{\rm dc}}{\dfrac{{V_{\rm in.pk}}^2}{\pi L_b (V_{\rm dc} + nV_o)} \displaystyle\int_0^{\pi} \frac{\sin^2(\omega t)}{1 - \dfrac{V_{\rm in.pk}}{V_{\rm dc} + nV_o} |\sin(\omega t)|} d\omega t}. \tag{38}$$

$L_e = 407\ \mu$H is calculated by substituting $n = 3$, $\mathrm{V_{pk}} = 100\sqrt{2}$ V, $V_{\rm dc} = V_{\rm pk}$ [V], $V_o = 48$ V and $L_b = 355\ \mu$H in (38). Fig. 6 shows the relationship between L_b and L_e for different values of turn ratio n. L_1 and L_m can be calculated from the following relation $1/L_e = (1/L_1) + (1/L_m)$. Therefore, if L_1 is equal to L_m, $L_1 = L_m = 815\ \mu$H is obtained.

E. Voltage Stress of Devices

In the proposed LED driver, the maximum voltage across S_1 is clamped to $2V_{\rm dc}$; the maximum voltage occurs for a very short time. Thus, the approximate average voltage stress on S_1 is assumed to $V_{\rm dc} + nV_o$. The other voltage and current stresses on the components of the proposed LED driver are shown in Table I.

F. Direct Power Transfer

In the conventional boost-flyback PFC converter, the input power is transferred to the dc-bus capacitor. And then, this stored energy is transferred to the load by the flyback dc–dc module. In the proposed LED driver, some of the input power is directly transferred to the load by the flyback dc–dc module with lossless snubber, and the remaining power is stored in the dc-bus capacitors.

From (34), the output power can be obtained by

$$P_{\rm out} = V_o I_o = \frac{nV_o {V_{\rm in.pk}}^2 D^2 T_s}{2\pi L_b} \times \int_0^{\pi} \frac{\sin^2(\omega t)}{V_{\rm dc} + nV_o - V_{\rm in.pk} |\sin(\omega t)|} d\omega t + \left(\frac{1}{4L_1} + \frac{1}{4L_m}\right) {V_{\rm dc}}^2 D^2 T. \tag{39}$$

Therefore, the directly transferred power, $P_{\rm direct}$, is expressed as follows:

$$P_{\rm direct} = P_{\rm out} - \left(\frac{1}{4L_1} + \frac{1}{4L_m}\right) {V_{\rm dc}}^2 D^2 T. \tag{40}$$

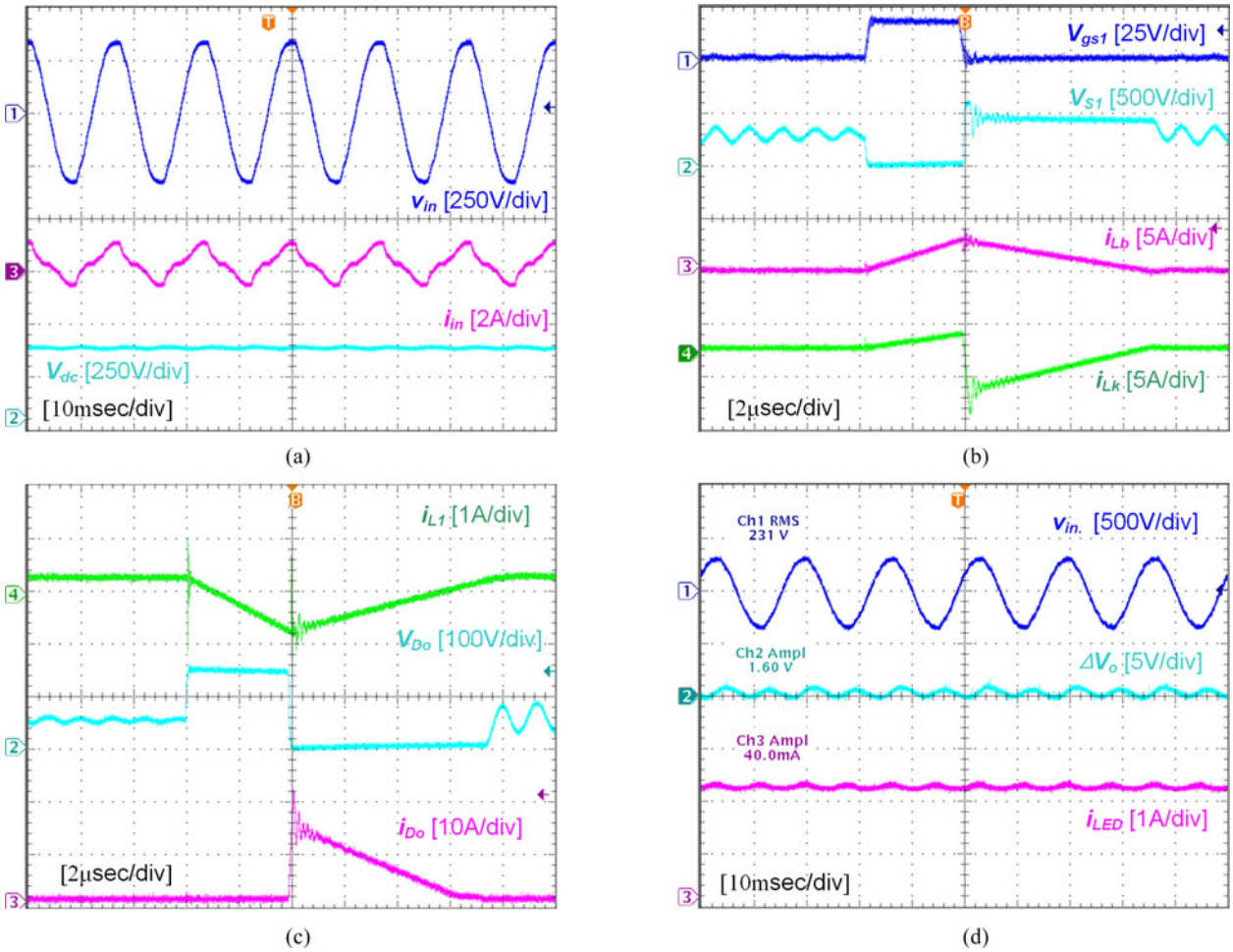

Fig. 9. Experimental waveforms at $v_{\rm in} = 230[V_{\rm ac}]$. (a) $v_{\rm in}$, $i_{\rm in}$, and $V_{\rm dc}$, (b) $v_{\rm gs1}$, v_{S1}, $i_{\rm Lb}$ and $i_{\rm Lk}$, (c) i_{L1},$v_{\rm Do}$, and $i_{\rm Do}$, (d) $v_{\rm in}$, ΔV_o and $i_{\rm LED}$.

By substituting $P_o = 100$ W, $n = 3$, $D = 0.45$, $V_{\rm dc} = V_{\rm pk} = 100\sqrt{2}$ V, $L_1 = L_m = 815$ μH, $T_s = 20$ μs, and $V_o = 48$ V into (40), the directly transferred power is calculated as 38.6503 W.

IV. Experimental Results

To verify the steady-state performance and theoretical analysis of the proposed single-switch ac–dc LED driver based on the boost-flyback PFC converter with a lossless snubber, a laboratory prototype with the following specifications is implemented and tested:

1) input line voltage range $v_{\rm in} = 100$–$230[V_{\rm ac}]$;
2) input line frequency $f_L = 60$ Hz;
3) output voltage $V_o = 48$ V;
4) output current $I_o = 2$ A;
5) output current ripple $\Delta I_o = 2[\%]$;
6) switching frequency $f_s = 50$ kHz;
7) measured THD 16.28[%] at $100[V_{\rm ac}]$, 24.62[%] at $230[V_{\rm ac}]$.

The selected parameters and components of the laboratory prototype, which are based on the above design specification, are listed in Table II. The laboratory prototype (proposed LED driver) circuit diagram and two linear constant-LED-current circuits are shown in Fig. 7. To drive the LED at a constant current, two linear constant-LED-current circuits [shown in Fig. 7(b)] are included; they drive at a current of 2 A (each driver provides $i_{\rm LED} = 1$ A).

Figs. 8(a) and 9(a) show the experimental waveforms of $v_{\rm in}$, $i_{\rm in}$, and $V_{\rm dc}$ at $100[V_{\rm ac}]$ and $230[V_{\rm ac}]$, respectively. These data show that a high power factor is achieved because the phase of the input current is similar to that of the input line voltage. However, $i_{\rm in}$ is not perfectly sinusoidal because this distortion depends on the ratio of $V_{\rm in.pk}/(V_{\rm dc} + nV_o)$; this distortion will be reduced because of the relatively high dc-bus voltage. Figs. 8(b) and 9(b) show the experimental waveforms of $v_{\rm gs1}$, v_{S1}, $i_{\rm Lb}$, and $i_{\rm Lk}$ at $100[V_{\rm ac}]$ and $230[V_{\rm ac}]$, respectively. These results show that L_b operates in DCM for PFC. At a high input voltage, the leakage inductor discharging time is shorter than the low input voltage condition because voltage across the leakage inductor is higher. Figs. 8(c) and 9(c) show the experimental waveforms of i_{L1}, $v_{\rm Do}$, and $i_{\rm Do}$ at $100[V_{\rm ac}]$ and $230[V_{\rm ac}]$, respectively. Because the output current $i_{\rm Do}$ is discontinuous, the reverse-recovery problem of the output diode is alleviated. Therefore, all of the inductors operate in DCM. Moreover, these results show that direct power transfer is achieved. Figs. 8(d) and 9(d)

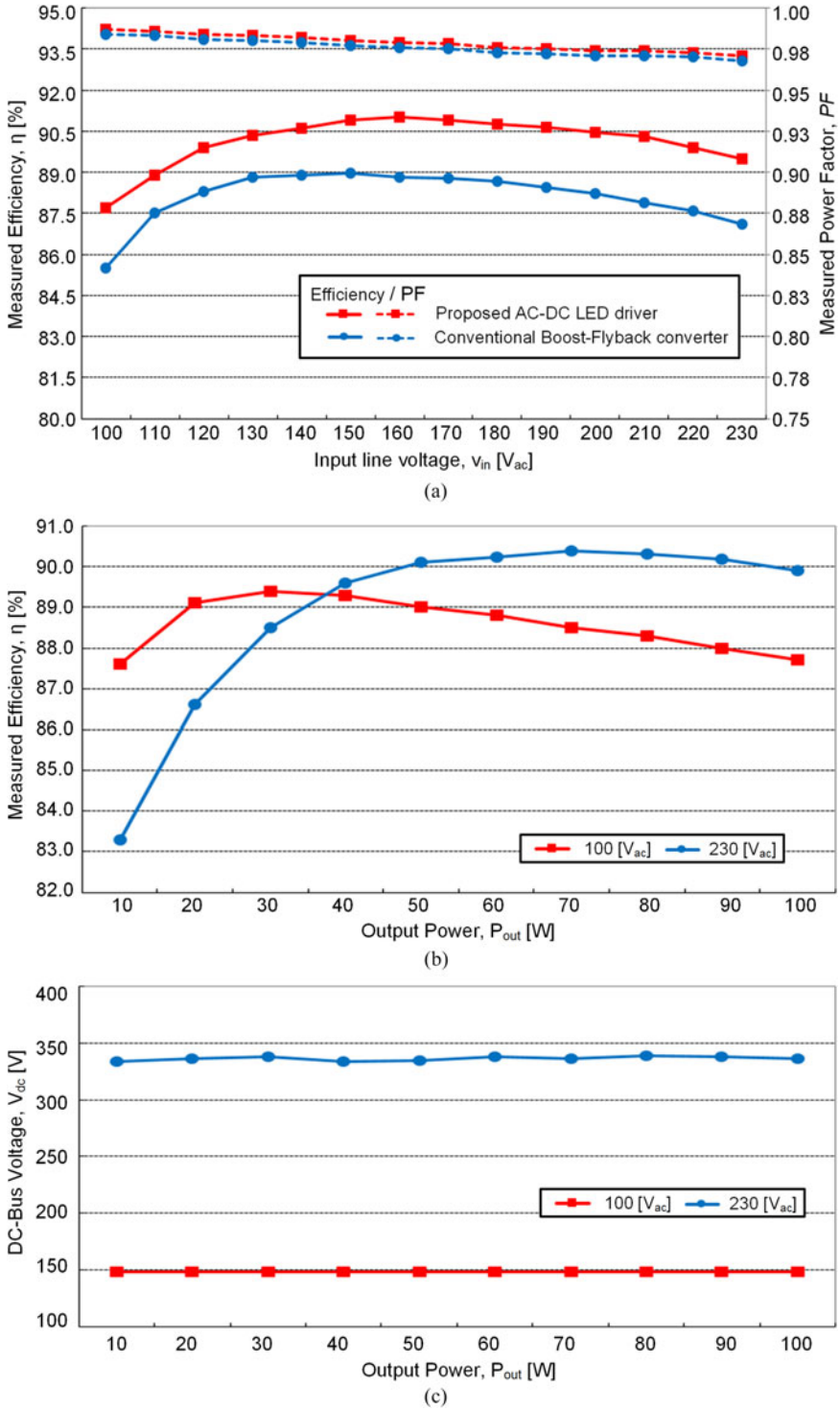

Fig. 10. Measured efficiency, power factor, and dc-bus voltage. (a) Efficiency and power factor according to input line voltage $v_{\rm in}$ at 100 W. (b) Efficiency under different output power P_o at 100[$V_{\rm ac}$] and 230[$V_{\rm ac}$]. (c) DC-bus voltage under different output power P_o at 100[$V_{\rm ac}$] and 230[$V_{\rm ac}$].

show the experimental waveforms of $v_{\rm in}$, ΔV_o, *and* $i_{\rm LED}$ at 100[$V_{\rm ac}$] and 230[$V_{\rm ac}$], respectively.

Fig. 10(a) presents a comparison between the efficiency and power factor of the proposed LED driver and those of the conventional boost-flyback PFC converter. The efficiency and power factor were measured at 100 W for different input line voltages. In the measured efficiency, the losses of two linear regulator are not included. To obtain a fair comparison, the conventional converter is designed with the same specifications and operating modes as the proposed LED driver. Because of the direct transfer of power and recycling of leakage inductor energy, the proposed LED driver achieves a higher efficiency than that of the conventional converter. The power factor of the proposed LED driver is similar to that of the conventional driver for the

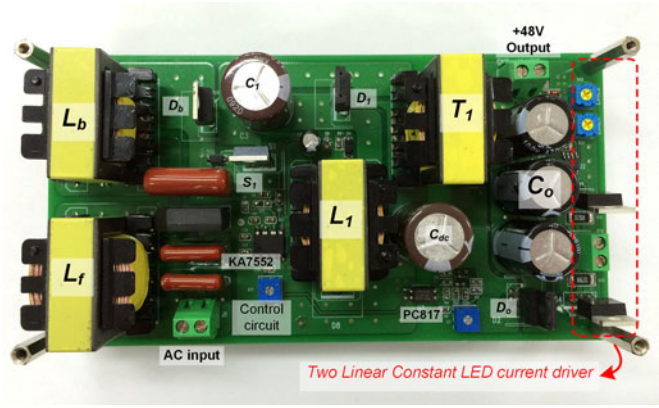

Fig. 11. Photograph of the prototype.

same PFC operation. However, because the snubber capacitor absorbs the leakage inductor's energy, the dc-bus voltage (which is the same as the snubber voltage in the prototype) is higher than that of the theoretical analysis. Therefore, the power factor of the proposed LED driver is slightly higher than that of the conventional converter. The efficiency and dc-bus voltage trajectory of the proposed LED driver under different output power P_o at 100[$V_{\rm ac}$] and 230[$V_{\rm ac}$] are shown in Fig. 10(b) and (c), respectively. Fig. 11 shows a photograph of the prototype.

V. Conclusion

A single-switch ac–dc LED driver based on a boost-flyback PFC converter with a lossless snubber has been proposed. Using the boost PFC circuit in DCM operation, a high power factor is achieved. In the dc–dc flyback circuit, because of the lossless snubber circuit, the peak voltage stress of the switch is clamped and the leakage inductor energy is recycled. The dc-bus capacitor is split into two capacitors (because the snubber capacitor is used). Additionally, a low-voltage-rating capacitor can be used because some of the input power at the boost inductor is directly conducted to the output. Therefore, the total efficiency is improved. The performance of an LED driver prototype has been experimentally evaluated at an output current of 2 A and an output voltage of 48 V.

References

[1] N. Chen and H. S.-H. Chung, "An LED lamp driver compatible with low- and high-frequency sources," *IEEE Trans. Power Electron.*, vol. 28, no. 5, pp. 2551–2568, May 2013.
[2] J. Choi, H.-S. Han, and K. Lee, "A current-sourced LED driver compatible with fluorescent lamp ballasts," *IEEE Trans. Power Electron.*, vol. 30, no. 8, pp. 4455–4466, Aug. 2015.
[3] Y.-L. Lin, H.-J. Chiu, Y.-K. Lo, and C.-M. Leng, "LED backlight driver circuit with dual-mode dimming control and current-balancing design," *IEEE Trans. Ind. Electron.*, vol. 61, no. 9, pp. 4632–4639, Sep. 2014.
[4] J.-K. Kim, J.-B. Lee, and G.-W. Moon, "Isolated switch-mode current regulator with integrated two boost LED drivers," *IEEE Trans. Ind. Electron.*, vol. 61, no. 9, pp. 4649–4653, Sep. 2014.
[5] J.-W. Yang and H.-L. Do, "High-efficiency ZVS AC-DC LED driver using a self-driven synchronous rectifier," *IEEE Trans. Circuits Syst. I, Reg. Papers*, vol. 61, no. 8, pp. 2505–2512, Aug. 2014.
[6] K. I. Hwu, Y. T. Yau, and L.-L. Lee, "Powering LED using high-efficiency SR flyback converter," *IEEE Trans. Ind. Appl.*, vol. 47, no. 1, pp. 376–386, Jan./Feb. 2011.
[7] S. Wang, X. Ruan, K. Yao, S.-C. Tan, Y. Yang, and Z. Ye, "A flicker-free electrolytic capacitor-less AC–DC LED driver," *IEEE Trans. Power Electron.*, vol. 27, no. 11, pp. 4540–4548, Nov. 2012.
[8] J. C. W. Lam and P. K. Jain, "A high power factor, electrolytic capacitor-less AC-input LED driver topology with high frequency pulsating output current," *IEEE Trans. Power Electron.*, vol. 30, no. 2, pp. 943–954, Feb. 2015.
[9] S. Jung and G.-H. Cho, "Transformer coupled recycle snubber for high efficiency offline isolated LED driver with on-chip primary-side power regulation," *IEEE Trans. Ind. Electron.*, vol. 61, no. 12, pp. 6710–6719, Dec. 2014.
[10] X. Wu, Z. Wang, and J. Zhang, "Design considerations for dual-output quasi-resonant flyback LED driver with current-sharing transformer," *IEEE Trans. Power Electron.*, vol. 28, no. 10, pp. 4820–4830, Oct. 2013.
[11] S.-C. Moon, G.-B. Koo, and G.-W. Moon, "A new control method of interleaved single-stage flyback AC–DC converter for outdoor LED lighting systems," *IEEE Trans. Power Electron.*, vol. 28, no. 8, pp. 4051–4062, Aug. 2013.
[12] Y. Hu, L. Huber, and M. M. Jovanovic, "Single-stage, universal-input AC/DC LED driver with current-controlled variable PFC boost inductor," *IEEE Trans. Power Electron.*, vol. 27, no. 3, pp. 1579–1587, Mar. 2012.
[13] Y. Jang, D. L. Dillman, and M. M. Jovanovic, "A new soft-switched PFC boost rectifier with integrated flyback converter for stand-by power," *IEEE Trans. Power Electron.*, vol. 21, no. 1, pp. 66–72, Jan. 2006.
[14] Y.-C. Li and C.-L. Chen, "A novel primary-side regulation scheme for single-stage high-power-factor AC–DC LED driving circuit," *IEEE Trans. Ind. Electron.*, vol. 60, no. 11, pp. 4978–4986, Nov. 2013.
[15] Y.-C. Li and C.-L. Chen, "A novel single-stage high-power-factor AC-to-DC LED driving circuit with leakage inductance energy recycling," *IEEE Trans. Ind. Electron.*, vol. 59, no. 2, pp. 793–802, Feb. 2012.
[16] C.-A. Cheng, C.-H. Chang, T.-Y. Chung, and F.-L. Yang, "Design and implementation of a single-stage driver for supplying an LED street-lighting module with power factor corrections," *IEEE Trans. Power Electron.*, vol. 30, no. 2, pp. 956–966, Feb. 2015.
[17] P. S. Almeida, H. A. C. Braga, M. A. D. Costa, and J. M. Alonso, "Offline soft-switched LED driver based on an integrated bridgeless boost-asymmetrical half-bridge converter," *IEEE Trans. Ind. Appl.*, vol. 51, no. 1, pp. 761–769, Jan./Feb. 2015.
[18] C.-A. Cheng, H.-L. Cheng and T.-Y. Chung, "A novel single-stage high-power-factor LED street-lighting driver with coupled inductors," *IEEE Trans. Ind. Appl.*, vol. 50, no. 5, pp. 3037–3045, Sep./Oct. 2015.

Sin-Woo Lee received the B.S. and M.S. degrees from the Seoul National University of Science and Technology, Seoul, South Korea, in 2014 and 2016, respectively, where he is currently working toward the Ph.D. degree in electronic engineering.

His research interests include power factor correction, ac–dc/dc–dc power converter, soft-switching power converters, renewable energy conversion, and LED lighting.

Hyun-Lark Do received the B.S. degree from Hanyang University, Seoul, South Korea, in 1999, and the M.S. and Ph.D. degrees in electronic and electrical engineering from the Pohang University of Science and Technology, Pohang, South Korea, in 2002 and 2005, respectively.

From 2005 to 2008, he was a Senior Research Engineer with the PDP Research Laboratory, LG Electronics, Inc., Gumi, South Korea. Since 2008, he has been with the Department of Electronic and Information Engineering, Seoul National University of Science and Technology, Seoul, where he is currently a Professor. His research interests include the modeling, design, and control of power converters, soft-switching power converters, resonant converters, PFC circuits, driving circuits for plasma display panels.